IOP Publishing Journal of Physics D: Applied Physics

J. Phys. D: Appl. Phys. **46** (2013) 305202 (7pp) doi:10.1088/0022-3727/46/30/305202

The production and evolution of atomic oxygen in the afterglow of streamer discharge in atmospheric pressure fuel/air mixtures

S J Pendleton[1], S Bowman[2], C Carter[3], M A Gundersen[1] and W Lempert[2]

[1] Pulsed Power Research Group, University of Southern California, Los Angeles, CA 90089, USA
[2] Michael A. Chaszeyka Non-Equilibrium Thermodynamics Laboratory, The Ohio State University, Columbus, OH 43210, USA
[3] Air Force Research Laboratory, Wright-Patterson Air Force Base, OH 45433, USA

E-mail: spendlet@usc.edu

Received 22 April 2013, in final form 7 June 2013
Published 2 July 2013
Online at stacks.iop.org/JPhysD/46/305202

Abstract

In this work two-photon absorption laser-induced fluorescence was used to measure oxygen atom (O) concentrations in streamer discharge afterglow in a variety of fuel/air mixtures in order to account for the O reaction pathways in transient plasma ignition. It is demonstrated that O atoms are generated in high concentration ($\sim 5 \times 10^{17}$ cm^{-3}) directly below the high-voltage anode in a point-to-plane geometry. The corresponding lifetimes in air were on the order of hundreds of microseconds. Fuel chemistry provides consumption pathways via chain branching reactions even without sustained combustion, and the corresponding O-atom lifetimes were much shorter than in air and dependent on the fuel concentration. At the richest conditions, corresponding to a fuel–air equivalence ratio of 2.4, O lifetimes were on the order a few microseconds or less. These experimental results are compared to modelling estimates in order to better understand the role of atomic oxygen in the chemical processes leading to ignition.

(Some figures may appear in colour only in the online journal)

1. Introduction and background

Streamer discharge results from the application to an electrode gap of a very short duration electrical pulse of much greater amplitude than the gas breakdown voltage. Known as transient plasma ignition (TPI), the use of streamers for ignition in combustion engines, holds great promise for improving performance. TPI has been tested to date in a variety of different ignition regimes including pulsed detonation engines (PDEs) and automobile engines, and experiments have already shown TPI to decrease ignition delay, increase flame speed, allow ignition of leaner mixtures, and increase net heat release in comparison to standard spark gap or arc ignition methods [1–4]. These improvements to combustion allow increasing power and efficiency in existing engines such as internal combustion engines, while enabling operational regimes previously unobtainable for experimental devices such as PDEs and scramjets (supersonic combustion ramjets) engines. Furthermore, mature pulse generation technology has already been successfully implemented into test engines [4–6].

A physical and chemical understanding of how the technology enhances combustion, however, lags behind the implementation and characterization of TPI in engines. TPI was initially assumed to be primarily a volumetric effect, but experimental work has shown ignition occurs in a spatially inhomogeneous manner with combustion improvements independent from electrode volume [5, 7, 8]. Developing a predictive understanding of the technology, thus allowing engine design to fully utilize its potential to enhance combustion, requires better understanding of the physics and chemistry of TPI.

It is to this end that we here report optical measurements of oxygen (O) atom concentrations in the afterglow of streamer discharge in fuel/air mixtures outside the limits of combustion.

Report Documentation Page

Form Approved
OMB No. 0704-0188

1. REPORT DATE	2. REPORT TYPE	3. DATES COVERED
02 JUL 2013		**00-00-2013 to 00-00-2013**

4. TITLE AND SUBTITLE	5a. CONTRACT NUMBER
The production and evolution of atomic oxygen in the afterglow of streamer discharge in atmospheric pressure fuel/air mixtures	5b. GRANT NUMBER
	5c. PROGRAM ELEMENT NUMBER
6. AUTHOR(S)	5d. PROJECT NUMBER
	5e. TASK NUMBER
	5f. WORK UNIT NUMBER
7. PERFORMING ORGANIZATION NAME(S) AND ADDRESS(ES) **Ohio State University,Michael A. Chaszeyka Non-Equilibrium Thermodynamics Laboratory,Columbus,OH,43210**	8. PERFORMING ORGANIZATION REPORT NUMBER
9. SPONSORING/MONITORING AGENCY NAME(S) AND ADDRESS(ES)	10. SPONSOR/MONITOR'S ACRONYM(S)
	11. SPONSOR/MONITOR'S REPORT NUMBER(S)

12. DISTRIBUTION/AVAILABILITY STATEMENT
Approved for public release; distribution unlimited

13. SUPPLEMENTARY NOTES

14. ABSTRACT

In this work two-photon absorption laser-induced fluorescence was used to measure oxygen atom (0) concentrations in streamer discharge afterglow in a variety of fueVair mixtures in order to account for the 0 reaction pathways in transient plasma ignition. It is demonstrated that 0 atoms are generated in high concentration (~5 x 1017 cm-3) directly below the high-voltage anode in a point-to-plane geometry. The corresponding lifetimes in air were on the order of hundreds of microseconds. Fuel chemistry provides consumption pathways via chain branching reactions even without sustained combustion, and the corresponding 0-atom lifetimes were much shorter than in air and dependent on the fuel concentration. At the richest conditions, corresponding to a fuel-air equivalence ratio of 2.4, 0 lifetimes were on the order a few microseconds or less. These experimental results are compared to modelling estimates in order to better understand the role of atomic oxygen in the chemical processes leading to ignition.

15. SUBJECT TERMS

16. SECURITY CLASSIFICATION OF:			17. LIMITATION OF ABSTRACT	18. NUMBER OF PAGES	19a. NAME OF RESPONSIBLE PERSON
a. REPORT **unclassified**	b. ABSTRACT **unclassified**	c. THIS PAGE **unclassified**	**Same as Report (SAR)**	**7**	

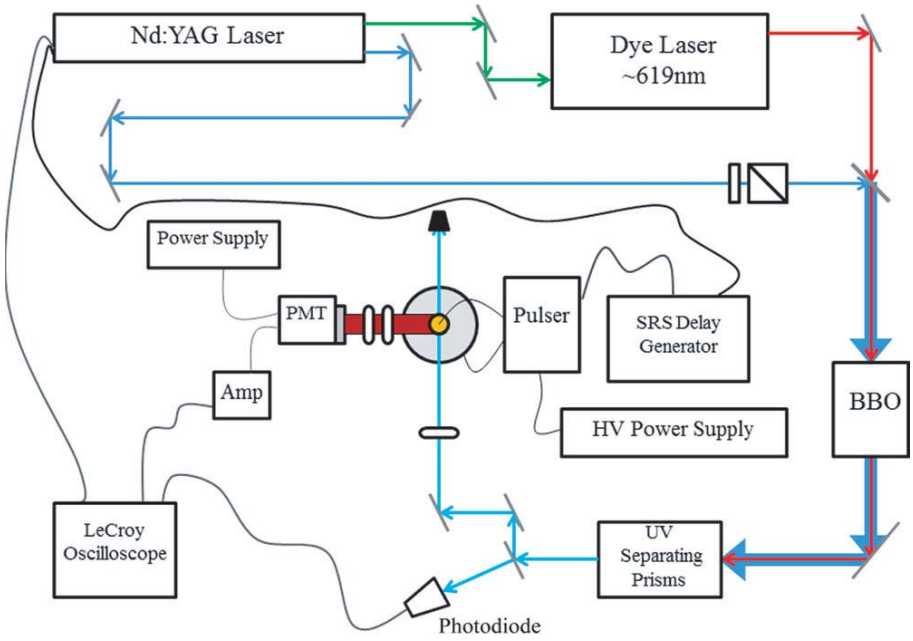

Figure 1. Experimental schematic of optical setup and discharge generation.

These results will elucidate the oxygen chemical pathways in the afterglow of the discharge and thus provide clues to the nature of the combustion improvements made by TPI.

2. Experiment

The experimental setup for these studies consists of a pulse generator and electrodes integrated into a flow-through premixed gas system coupled to an optical setup for conducting two-photon absorption laser-induced fluorescence (TALIF), as shown in figure 1.

A pulse generator nearly identical to that described in [6] was used for these experiments, with the silicon-controlled rectifier (SCR) replaced by a bank of commercial insulated-gate bipolar transistors (IGBTs) in parallel for the purposes of timing precision and repetition rate; the pulse-forming network was otherwise unchanged. This pulse generator produces a Gaussian-like voltage waveform with a controllable amplitude of 10–60 kV (20 ns full width at half maximum (FWHM)). Sample voltage and current traces of the discharge in air are shown in figure 2, employing a Northstar PVM-5 voltage probe (80 MHz bandwidth), a Pearson 6223 current probe (200 MHz bandwidth), and a LeCroy Wavepro WavePro 725Zi oscilloscope with 2.5 GHz bandwidth. For the purposes of maintaining consistency with previous work and within this work, a 16.5 kV positive pulse amplitude was used for all measurements reported here; this corresponds to a 19.5 A peak current and 4.75 mJ energy input per pulse. All data were recorded at a pulse repetition frequency of 10 Hz to match the optimal laser repetition rate.

TPI electrodes have traditionally used a coaxial design with a centre threaded rod high-voltage anode and outer grounded cathode due to the cylindrical symmetry inherent to many engine applications [1–3]. A fully three dimensional,

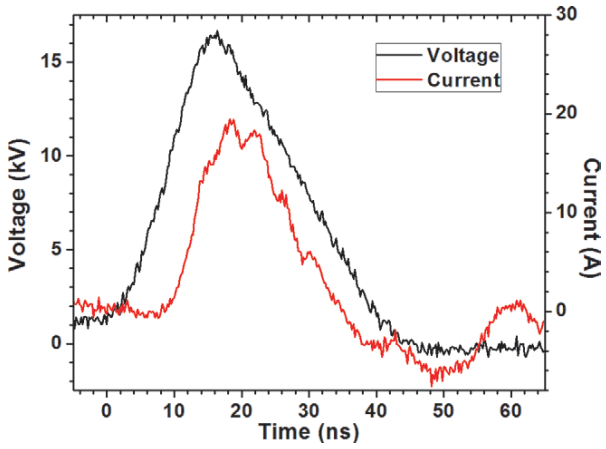

Figure 2. Voltage and current traces for the discharge in air.

multi-streamer electrode geometry, however, is challenging for laser-based diagnostics, and thus the electrodes were modified to a point-to-plane geometry for the purposes of these experiments, with a steel needle with tip curvature of radius 75 μm as the anode and the sintered bronze surface of a McKenna burner (fabricated by Holthius and Associates) as the grounded cathode. Current was monitored using a Pearson 6223 current probe in line with the high-voltage cable supplying the anode. The 8 mm gap used in previous TPI experiments was retained for the point to plane geometry. As previous experiments demonstrate that ignition occurs in the region of high E/N (where E is the electric field and N the total gas number density) near the anode, experiments were conducted in a cube 250 μm on edge directly below to the anode tip, as shown in figure 3 [8]. This region of interest (ROI), defined optically as described below, was chosen to

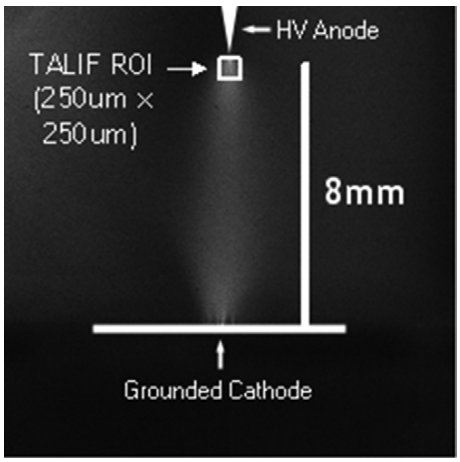

Figure 3. Image of discharge showing spatial ROI.

approximately match the diameter of the discharge directly below the anode as determined by images of spontaneous plasma emission.

Gas compositions and flow rates were maintained with Tylan mass flow controllers. Flow rate was regulated to produce a gas speed of 10 cm s^{-1} to ensure complete recycling of gas volume in the discharge from shot to shot at the 10 Hz laser repetition rate while maintaining a quasi-quiescent environment. The McKenna burner with a sintered bronze flameholder radius of 3 cm was used to deliver a pre-mixed gas flow to the discharge region as well as to serve as the grounded anode for the discharge; the needle anode was mounted 8 mm above the centre of the burner in order to isolate it from the edge of the flow and eliminate the need for a nitrogen co-flow. For all gas mixtures, filtered facility compressed air was used to minimize moisture content at less than 2% relative humidity. Ethylene (C_2H_4), methane (CH_4), and propane (C_3H_8), of purity 99.985%, 99.99% and 99.99%, respectively, were used for fuel/air mixtures. These fuels were chosen for comparison with previous TPI experiments [5–8]. The fuel–air equivalence ratio was chosen to be just outside of limits of flame stabilization for this system, with an extra point at half the lean limit, in order to simulate the conditions of ignition without introducing the complication of unquenched combustion chain reactions and flame development. The fuel lean and rich combustion limits were determined experimentally specifically for this setup.

The time delay between the discharge and the laser was controlled with a Stanford Research Systems DG-645 digital delay generator and verified with an oscilloscope using a ThorLabs DET10A photodiode to collect laser scatter and the discharge current; the beginning of the current rise was specified as $t = 0$ for all work presented here. Since the repetition rate of the laser is limited to 10 Hz, every discharge was probed by the laser only once; thus, every time delay was measured in a separate discharge event and time sequences were constructed from the data in post processing rather than in real time.

The laser was passed through the electrode gap directly beneath the anode. The position of the burner/electrode with respect to the laser beam was maintained with a three-axis Newport MM300 motion controller/driver. The height of the beam with respect to the electrode was adjusted so that it could be as close to the electrode as possible without producing measurable scattering. In order to prevent optical saturation effects, the waist of the focused laser beam was located several cm behind the measurement volume. The width of the beam passing through the discharge was measured to be 250 μm (FWHM); the height and depth of the ROI are thus 250 μm.

The optical setup for TALIF uses an injection-seeded Continuum Surelite III Q-switched Nd : YAG laser, with the 532 nm second harmonic output used to pump a Continuum ND6000 tunable dye laser. The Nd : YAG the third harmonic beam (355 nm) was then frequency mixed with the 619.84 nm dye laser beam in a BBO crystal to generate the 225.7 nm beam necessary to pump the O-atom transition between the ground 2p ^{3}P state and the excited 3p ^{3}P state. It should be noted at higher laser intensities the excited atom may be ionized by a third 225.7 nm photon, but for the laser fluences used in this experiment, this effect is negligible. The fluorescence signal at 844.87 nm resulting from radiative decay to the 3s ^{3}S state was 1 : 1 imaged onto a vertical slit (with a 250 μm width) placed in front of a Hamamatsu R3896 photomultiplier tube (PMT); the fluorescence was isolated from Rayleigh scattering (and other background radiation) using an 80 nm bandpass filter, centred at 850 nm, that was placed over the PMT housing entrance. Thus, the probe dimensions were defined in the beam propagation dimension by the 250 μm slit width and in the vertical and radial dimensions by the 250 μm laser beam width. This laser probe size was confirmed by translating the discharge in the radial direction using the motion controller. The PMT fluorescence signal was amplified by 25 times and recorded with a LeCroy WavePro 7100A oscilloscope. This oscilloscope was also used to integrate the signal over the time of the laser pulse and to calculate the average and variance over thousands of laser shots; due to high variation of the signal, 3000 shots were taken for each data point. A photodiode was used to collect laser scatter, and the PMT signal was normalized by the square of this scattered intensity in order to account for laser intensity variation. For all data the mean and standard deviation were recorded for 3000 discharge events, and the uncertainty shown in plots is derived by combining the standard deviation of the mean of all measured quantities using standard error propagation techniques. The apparatus and procedure are described in more detail in [9, 10].

Conversion from relative O-atom population to absolute number density is made by comparison of identical measurements made in a xenon gas cell of known concentration with laser wavelength shift to 224.31 nm to pump the two-photon $5p^6\,{}^1S_0$ to $6p'[3/2]_2$ transition in xenon atoms [11]. The resulting fluorescence at 834.91 nm due to relaxation to the $6p'[3/2]_2$ state is again collected using the identical detector setup [12]. Conversion from known number density of xenon N_{Xe} to number density of O atoms uses the following expression:

$$N_O = \frac{S_O}{S_{Xe}} g_{ND} \frac{a_{21}\,(Xe)}{a_{21}\,(O)} \left(\frac{\sigma^{(2)}\,(Xe)}{\sigma^{(2)}\,(O)}\right) \left(\frac{\upsilon_O}{\upsilon_{Xe}}\right)^2 \frac{1}{F_O(T)} N_{Xe} \quad (1)$$

where the S_i are the observed signals normalized by the square of the laser intensity, $a_{21} = A_{21}/(A_{21}+Q)$ are the fluorescence quantum yields (where A_{21} and Q are the spontaneous emission and quenching rates, respectively), $\sigma^{(2)}$ are the two-photon absorption cross sections, v_O/v_{Xe} is the laser frequency correction due to using equivalent energy and thus a different number of photons per excitation pulse, and $F_O(T)$ is the Boltzmann factor for the lower level of the O-atom ground state [9]. The a_{21} were calculated assuming an upper bound on the quenching rate for O at atmospheric pressure using the following quenching coefficients:

(1) $O + O_2$ with $k \approx 9.4 \times 10^{-10}$ cm^3 s^{-1} [12],
(2) $O + H_2$ with $k \approx 10.9 \times 10^{-10}$ cm^3 s^{-1} [12],
(3) $O + CH_4/C_2H_4/C_3H_8$ with $k \approx 5.5 \times 10^{-10}$ cm^3 s^{-1} [13],
(4) $O + H_2O$ with $k \approx 4.9 \times 10^{-9}$ cm^3 s^{-1} [13],
(5) $O + N_2$ with $k \approx 5.9 \times 10^{-10}$ cm^3 s^{-1} [11],
(6) $Xe + Xe$ with $k \approx 9.4 \times 10^{-10}$ cm^3 s^{-1} [12].

In order for equation (1) to be true, all other optical factors must remain constant including PMT gain voltage; in order to maintain this consistency, the xenon cell was substituted directly for the discharge in the beam path and a neutral density filter of factor g_{ND} was used in order to reduce the xenon fluorescence signal to within the linear operational region of the PMT while keeping the gain voltage constant. While the xenon cell provides a larger volume than the discharge from which to collect fluorescence, the sample volume was approximately the same as that used for O-atom measurements, due to the limits placed on the laser probe region. Temperatures for $F_O(T)$ were taken from recent coherent anti-Stokes Raman spectroscopy (CARS) measurements performed under identical mixture and discharge conditions [14], with extrapolation or interpolation at some values of time delay.

3. Results

Before optical measurements may be reported, it is necessary to fully characterize the discharge. Voltage and current traces were recorded and analysed for each gas mixture to quantify any changes in the electrode impedance. Despite noticeable macroscopic differences in various mixtures—the discharge pulses in richer mixtures were audibly louder than those in leaner mixtures for all three fuels—the measured electrical characteristics remained essentially identical with no more than 5% variation between any two mixtures in pulse width, peak current, peak voltage and energy delivered. A more complete electrical and optical characterization is reported in [14].

TALIF measurements of O number density in air are shown in figure 4. For the purposes of clarity, uncertainty—based on the standard deviation of the mean taken from 3000 shots, with variations in laser energy, TALIF signal, and Xe signal combined using standard error propagation techniques—is shown only on a single point but is representative of the value for all the points of that sequence.

O number densities measured in C_2H_4/air, CH_4/air and C_3H_8/air mixtures are shown in figures 5–7, respectively. As is the case with pure air, uncertainty, based on the standard

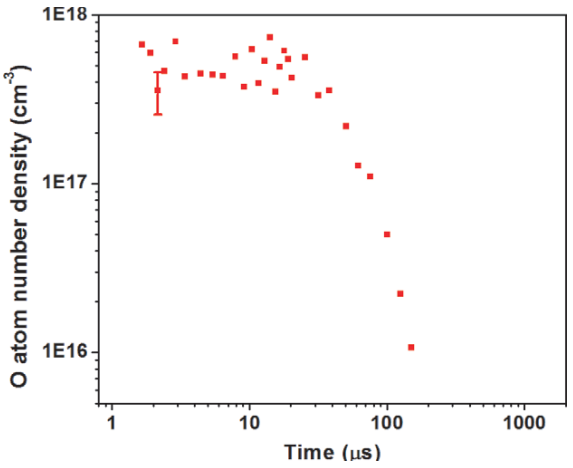

Figure 4. TALIF measurements of O number density in air at atmospheric pressure versus delay time from discharge initiation.

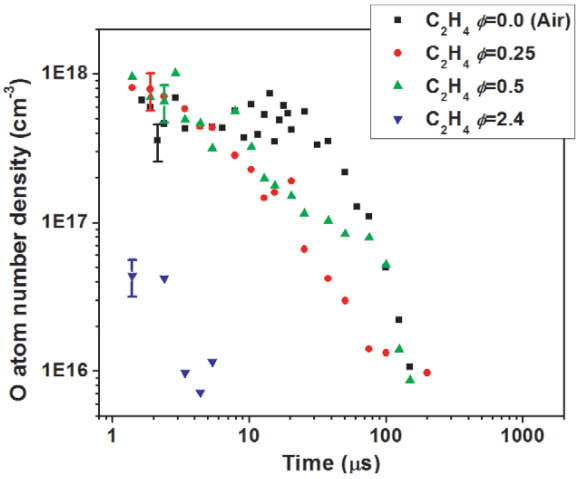

Figure 5. TALIF measurements of O number density in C_2H_4/air mixtures versus delay time from discharge initiation.

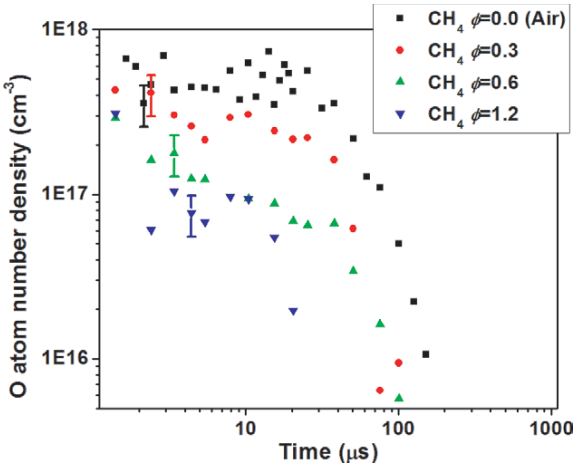

Figure 6. TALIF measurements of O number density in CH_4/air mixtures versus delay time from discharge initiation.

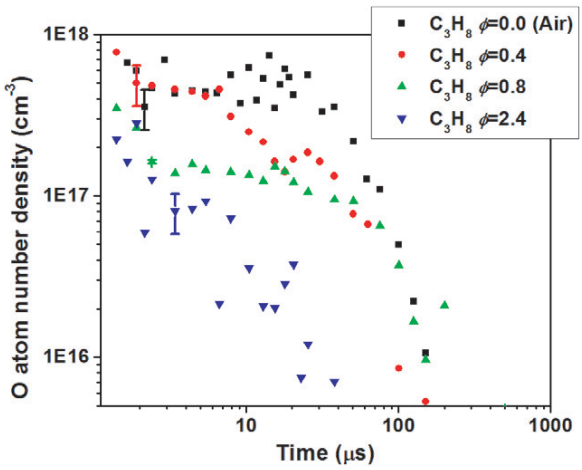

Figure 7. TALIF measurements of O number density in C_3H_8/air mixtures versus delay time from discharge initiation.

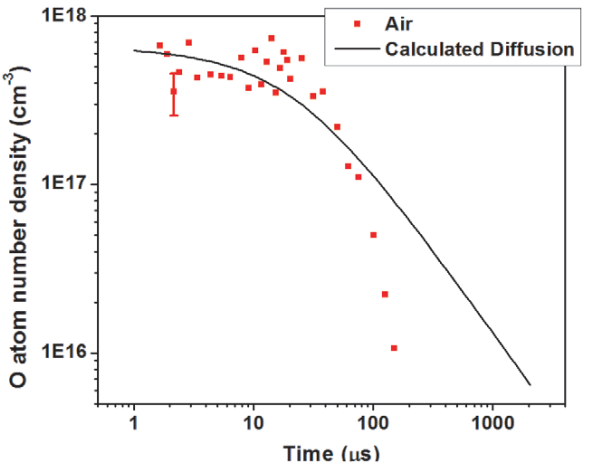

Figure 8. Calculated decay due to diffusion shown with measured O-atom concentration measured in pure air.

deviation of the mean taken from 3000 shots, is shown only on a single point for each time sequence with the displayed uncertainty applicable to all points for the rest of its sequence.

4. Discussion

Examination of O number density in pure air (figure 4) yields the result that O concentration is high shortly after the discharge, corresponding to a dissociation fraction of O_2 equal to ~0.18 assuming atmospheric pressure and rotational/translational temperature of ~1000 K, as determined in previously reported CARS measurements [13]. It can also be seen that the O number density remains approximately constant until ~40–50 μs after the discharge pulse, at which point it rapidly decays, dropping below the measurable threshold by ~200 μs. A kinetic analysis shows that the primary loss mechanism for atomic oxygen in air under these conditions is the three body recombination process, $O + O + M \rightarrow O_2 + M$, where M is either N_2 or O_2 (Note that at these relatively high temperatures ozone production due to $O + O_2 + M \rightarrow O_3 + M$ is negligible due to the fast rate of the reverse reaction). Using rate data from [15], the specific rate coefficient k for N_2 as third body collision partner at $T = 1000$ K is $k \approx 5 \times 10^{-34}$ cm^6 s^{-1}, corresponding to a half-life, $\tau = 1/k[N_2][O]$, equal to ~500 μs, an order of magnitude longer than the observed ~50 μs value. To explore possible explanations for this difference, the rate of decay of O atoms out of the ROI was estimated assuming that an initially uniform cylindrical distribution of O ($r \leqslant 0.125\,\mu$m) diffuses into an infinite medium. Diffusion of a trace amount of O in a background of N_2 was assumed, and the binary diffusion coefficient was derived using the measured temperatures from [14] and standard gas diffusion equations [16, 17]. A coupled simulation of the laser excitation process then provided an effective sampling volume; values for the two-photon-excitation probe size were then matched to the experimental values (for beam size and limiting aperture). This calculation shows a much reduced rate of fall-off in O compared to than shown in figure 4, as plotted in figure 8, although the drop in O corresponding to a reduction of the initial concentration by a factor of $(1/e)^2$ is predicted to be ~100 μs which is in reasonable agreement with the data. Another likely explanation is that due to the high energy loading of the filament, the discharge induces bulk convection of the gas out of the ROI that causes the observed rapid decay in signal.

Considering figure 5 it can be clearly seen that introduction of C_2H_4, even at relatively low equivalence ratio, results in a rapid increase in O consumption. While a full kinetic analysis is beyond the scope of this paper, some insight can be drawn from simple consideration of some important O loss processes. It is stressed that the analysis is not meant to provide a quantitative comparison with the data, as under these conditions the full chemistry, in particular chain branching and propagation is rather complicated, but rather to illustrate that O kinetics in the presence of fuel is predicted to be much faster than for air.

In the presence of C_2H_4, O is initially lost due to the parallel processes of:

(1) $O + C_2H_4 \rightarrow CH_3 + HCO$ with $k \approx 1.25 \times 10^{-11}$ cm^3 s^{-1} and
(2) $O + C_2H_4 \rightarrow CH_2CO + H$ with $k \approx 6.7 \times 10^{-12}$ cm^3 s^{-1}, both at $T = 1500$ K [14, 18].

The higher temperature is based on previous reported temperature measurements using CARS [14]. The corresponding O-atom half-life, $\tau = \ln(2)/k_{tot}\,[C_2H_4]$, assuming that the initial C_2H_4 concentration is much larger than that of O, is ~0.3 μs. However, for $\varphi = 0.25$ the initial C_2H_4 concentration at $P = 1$ bar and $T = 1500$ K is ~1.3×10^{17} cm^{-3} which is in fact a factor of ~4–6 less than the initial O concentration, which would tend to reduce the rate of decay due to these two processes. Note that under fuel rich conditions, where initial C_2H_4 concentration exceeds that of O, the observed rate of O-atom decay is much faster due, presumably, to both the absolute C_2H_4 being larger (increasing the reaction rate) and the fact that the C_2H_4 concentration

exceeds the initially formed O concentration. It should be noted that these O atom-consuming reactions above are chain branching reactions responsible, ultimately, for the runaway heat release of combustion.

A similar analysis can be performed for the CH_4 data in figure 6. In this case the primary loss processes for O are:

(1) $O + CH_4 \rightarrow OH + CH_3$, with $k = 7 \times 10^{-13}\,cm^3\,s^{-1}$,
(2) $O + CH_3 \rightarrow H + CH_2O$, with $k = 8.4 \times 10^{-11}\,cm^3\,s^{-1}$ and
(3) $O + CH_3 \rightarrow H + H_2 + CO$ with $k = 5.6 \times 10^{-11}\,cm^3\,s^{-1}$, all at $T = 1000\,K$ [14, 18].

Note that for CH_4 dissociation fraction of order 1% the rate of O-atom loss due to reaction with the methyl radical (CH_3) is comparable to that for reaction with CH_4. Considering only the CH_4 reaction pathway and a CH_4 number density at $P = 1$ bar, $T = 1000\,K$ and $\varphi = 0.6$ ($[CH_4] = 4 \times 10^{17}\,cm^{-3}$), the predicted O-atom half-life is $\sim 2.2\,\mu s$. Assuming 1% CH_4 dissociation to $H + CH_3$ and ignoring any coupling between the kinetic processes results in a total half-life from the three parallel processes of $\sim 0.8\,\mu s$. Both values are in reasonable accord with the measurements (figure 6, green triangles), which indicate a half-life of about 1–2 μs.

Finally, for C_3H_8 the principal O loss process is $O + C_3H_8 \rightarrow C_3H_7 + OH$ where the C_3H_7 radical can be formed in two isomeric configurations with total rate coefficient $k \approx 3 \times 10^{11}\,cm^3\,s^{-1}$ at $T = 1500\,K$ [14, 18]. At $P = 1$ bar, $T = 1500\,K$, and $\varphi = 0.8$ and 2.4 the initial C_3H_8 concentrations are $1.7 \times 10^{17}\,cm^{-3}$ and $4.7 \times 10^{17}\,cm^{-3}$, respectively, and corresponding predicted half-lives of 0.14 and 0.05 μs. These values are not unreasonable based on the data points in figure 7, but the specific values are near or below our detection limit for time (after the discharge).

5. Conclusion

The results of a comprehensive set of two-photon absorption laser-induced fluorescence measurements, describing the temporal evolution of O-atom concentration in quasi-quiescent C_2H_4/air, CH_4/air and C_3H_8/air mixtures outside the limits of sustained combustion (at atmospheric pressure), were presented and analysed for a point-to-plane nanosecond streamer discharge similar to that used for transient plasma ignition (TPI). For this purpose, O-atom fluorescence signals were calibrated, to derive absolute concentration, through the use of companion two-photon absorption laser-induced fluorescence measurements of Xe. In the probe region, directly below the high-voltage anode, it was shown that O concentration is quite high in the afterglow of the discharge, $[O] \sim 5 \times 10^{17}\,cm^{-3}$, equalling a dissociation mole fraction of roughly 18% in air. The rate of O-atom decay in air is found to be approximately ten times faster than that attributed to three body recombination reactions, which is the principal loss mechanism at the relatively high temperature conditions of the filament of 1000 K. Mass diffusion and/or convection are considered likely explanations for the discrepancy. The addition of fuels to the gas mixture decreased the maximum observed mole fraction, shortened the duration of the high concentration plateau, and increased the rate of decay. For all fuel/air mixtures, the amplitude of these changes increased monotonically with the concentration of fuel. The changes in O-atom behaviour due to fuels are attributed to chain branching reactions which are much more rapid than O-atom recombination. Further experiments are necessary to quantify the spatial distribution of O atoms as well as the production of intermediate reactive species in order to better understand the physics and chemistry of TPI. In addition, future experiments will probe varying discharge parameters including pulse amplitude and polarity in a spatial mapping of species density.

Acknowledgments

The authors would like to thank Igor Adamovich for discussions on chemical kinetics. In addition, the authors would like to thank the Air Force Office of Scientific Research MURI program in Plasma Assisted Combustion—Chiping Li technical monitor, the Propulsion Directorate's Summer Research Fellowship, the Office of Naval Research, NumerEx LLC and the National Science Foundation—Steven Gitomer technical monitor for support of this research.

References

[1] Cathey C D, Tao T, Shiraishi T, Urushihara T, Kuthi A and Gundersen M A 2007 Nanosecond plasma ignition for improved performance of an internal combustion engine *IEEE Trans. Plasma Sci.* **35** 1664–8
[2] Liu J, Wang F, Li G, Kuthi A, Gutmark E J, Ronney P D and Gundersen M A 2005 Transient plasma ignition *IEEE Trans. Plasma Sci.* **33** 326–7
[3] Wang F, Liu J B, Sinibaldi J, Brophy C, Kuthi A, Jiang C, Ronney P and Gundersen M A 2005 Transient plasma ignition of quiescent and flowing air/fuel mixtures *IEEE Trans. Plasma Sci.* **33** 844–9
[4] Shiraishi T, Urushihara T and Gundersen M 2009 A trial of ignition innovation of gasoline engine by nanosecond pulsed low temperature plasma ignition *J. Phys. D: Appl. Phys.* **42** 135208
[5] Singleton D R, Sinibaldi J O, Brophy C M, Kuthi A and Gundersen M A 2009 Compact pulsed-power system for transient plasma ignition *IEEE Trans. Plasma Sci.* **37** 2275–9
[6] Singleton D R, Kuthi A, Sanders J M, Gundersen M A, Simone A and Pendleton S J 2011 Low energy compact power modulators for transient plasma ignition *IEEE Trans. Dielectr. Electr. Insul.* **18** 1084–90
[7] Cathey C, Cain J, Wang H, Gundersen M A, Carter C and Ryan M 2008 OH production by transient plasma and mechanism of flame ignition and propagation in quiescent methane–air mixtures *Combust. Flame* **154** 715–27
[8] Singleton D, Pendleton S J and Gundersen M A 2011 The role of non-thermal transient plasma for enhanced flame ignition in C_2H_4–air *J. Phys. D: Appl. Phys.* **44** 022001
[9] Uddi M, Jiang N, Mintusov E, Adamovich I V and Lempert W R 2009 Atomic oxygen measurements in air and air/fuel nanosecond pulse discharges by two photon laser induced fluorescence *Proc. Combust. Inst.* **32** 929–36
[10] Bowman S, Adamovich I V and Lempert W 2012 Atomic oxygen measurements in $O_2(a\,^1\Delta_g)$ injected nonequilibrium plasmas by two photon absorption

laser induced fluorescence *50th AIAA Aerospace Sciences Meeting (Nashville, TN)*

[11] Niemi K, Gathen V S-v d and Dobele H F 2001 Absolute calibration of atomic density measurements by laser-induced fluorescence spectroscopy with two-photon excitation *J. Phys. D: Appl. Phys.* **34** 2330

[12] Niemi K, Gathen V S-v d and Dobele H F 2005 Absolute atomic oxygen density measurements by two-photon absorption laser-induced fluorescence spectroscopy in an RF-excited atmospheric pressure plasma jet *Plasma Sources Sci. Technol.* **14** 375

[13] Bittner J, Kohse-Höinghaus K, Meier U and Just T 1988 Quenching of two-photon-excited H(3s,3d) and O(3p $^3P_2$,1,0) atoms by rare gases and small molecules *Chem. Phys. Lett.* **143** 571–6

[14] Pendleton S J, Montello A, Carter C, Lempert W and Gundersen M A 2012 Vibrational and rotational CARS measurements of nitrogen in afterglow of streamer discharge in atmospheric pressure fuel/air mixtures *J. Phys. D: Appl. Phys.* **45** 1–8

[15] Kossyi I A, Kostinsky A A M A Yu and Silakov V P 1992 Kinetic scheme of the nonequilibrium discharge in nitrogen–oxygen mixtures *Plasma Sources Sci. Technol.* **1** 207–20

[16] Carslaw H S and Jaeger J C 1959 *Conduction of Heat in Solids* 2nd edn (Oxford: Clarendon) p 260

[17] Kee R J *et al* 2000 CHEMKIN Collection, Release 3.6, Reaction Design, Inc. San Diego, CA

[18] Wang H, You X, Joshi A V, Davis S G, Laskin A, Egolfopouolos F and Law C K 2007 USC Mech Version II. High-Temperature Combustion Reaction Model of H2/CO/C1-C4 Compounds, May 2007 Available: http://ignis.usc.edu/USC_Mech_II.htm